Investigating fission distribution behavior under various homogenization techniques for asymmetrical fuel assemblies and different reflector equivalence methods

Kevin Frohlicher, Vivian Salino, Alain Hebert

Annals of Nuclear Energy 157 (2021) 108221

Contents lists available at ScienceDirect

Annals of Nuclear Energy

journal homepage: www.elsevier.com/locate/anucene

Investigating fission distribution behavior under various homogenization techniques for asymmetrical fuel assemblies and different reflector equivalence methods

Kévin Fröhlicher [a], Vivian Salino [a,b], Alain Hébert [a,*]

[a] Polytechnique Montréal, C.P 6079 succ. "Centre-Ville", Montréal, Qc. H3C 3A7, Canada
[b] Institut de Radioprotection et de Sûreté Nucléaire, 31 Avenue de la Division Leclerc, 92260 Fontenay-aux-Roses, France

ARTICLE INFO

Article history:
Received 16 September 2020
Received in revised form 9 January 2021
Accepted 21 February 2021
Available online xxxx

Keywords:
Reactor physics
BEAVRS
Full-core calculations
DRAGON5 code
Assembly homogenization

ABSTRACT

This article provides an analysis of the impact of asymmetrical assemblies homogenization and reflector modeling methods over the fission distribution, based on the first startup of the BEAVRS benchmark v2.0.2, in Hot Zero Power state (HZP). We use a classical two-step simulation with the deterministic codes DRAGON5 and DONJON5. First a transport calculation is performed with DRAGON5 on fuel assemblies, based on previous work conducted at the *Polytechnique Montréal*. Then, the complete core calculation is done with DONJON5 using a two-group energy mesh, in diffusion theory. The fission rates are calculated using DONJON5 and compared to the in-core detectors data provided in the BEAVRS benchmark. Discrepancies between the simulation and radial adjusted measurements present a Root Mean Square error (RMS) discrepancy of $\simeq 4.5\%$ (with relative errors lower than 10%). The results show the necessity to consider heterogeneity when it comes to model assemblies without central symmetry.

1. Introduction

Whether in the context of safety studies or design, numerical simulations make it possible to predict the neutronic behavior of a reactor over a comprehensive range of configurations. Depending on the intended objective, different numerical methods are available. Stochastic or Monte Carlo methods can provide, with sufficient sampling, very accurate results (only errors related to nuclear data and statistical uncertainties remain) but this accuracy is associated with prohibitive calculation costs for industrial purposes. Deterministic methods, on the contrary, make it possible to produce fast results, subject to simplifying assumptions which can degrade the results.

For industrial type of analysis, the deterministic approach was chosen for its celerity. Although complete core calculation is possible in transport theory (Park et al., 2020), the associated computation costs remain substantial for industrial-type calculations (can be up to tens of hours for a multi-thread calculation Fröhlicher, 2019; Vidal et al., 2020). A two-step approach, modeling an assembly in an infinite medium, in transport theory, followed by a core calculation using the diffusion approximation (Darnowski and Pawluczyk, 2019; Bahadir, 2020; Leppänen et al., 2014; Taforeau and Salino, 2016), therefore remains the preferential method for such applications. The goal of the lattice step (transport calculation) is to produce homogenized and condensed few energy groups cross section libraries in order to characterize the modeled media in the core calculation.

The following study relates to the validation of the capabilities of the DRAGON5 and DONJON5 codes (Marleau et al., 2018; Hébert et al., 2019) to produce satisfactory results for the fission rates within the reactor core. The DRAGON5 code provides several solvers for the neutron transport equation in forms of modules. It allows the solving of neutron transport problems over a one- or two-dimension geometry with different boundary conditions available. As for the DONJON5 code, it is based on TRIVAC's diffusion and SP_n solvers (Hébert, 1987), and allows the modeling of more complex core problems thanks to additional modules such as THM: for simplified thermal–hydraulics simulation. The lattice calculations used in this study are based on the computational schemes of Canbakan and Hébert (2015) and are similar to the REL2005 schemes of (Vidal et al., 2007). A B_1 leakage model as well as an homogenization and condensation procedure have been added to the pre-existing double level scheme, in order to create efficient multi-group cross section libraries for core calculation. The two-step flux calculation in this phase takes advantage of the accuracy of the Method of Characteristics (MOC) on a refined

* Corresponding author.
E-mail address: alain.hebert@polymtl.ca (A. Hébert).

https://doi.org/10.1016/j.anucene.2021.108221
0306-4549/

geometry for an affordable calculation cost over the collision probability method (Hébert, 2020).

In order to validate the calculation scheme on an industrial reactor geometry with asymmetrical assemblies, the modeling was applied to the reactor described in the BEAVRS benchmark (Horelik et al., 2013). The results presented relate to the fission distribution of the Hot Zero Power (HZP) configuration of the first operating cycle. The comparison of the differences between the response of the detectors modeled in DONJON5 and the data available in the benchmark was made for different reflector models as well as for several different homogenization of asymmetrical assemblies. The module `IDET` recently developed in DONJON5, and further described in Section 5.3, allows the calculation of fission rates at precise points in the core, for a cartesian configuration.

The results were compared with the detector responses given in the BEAVRS benchmark, as well as with the corrected data (removing the azimuthal tilt) presented in version 2.0.2 of the benchmark, released on April 11, 2018, by the Massachusetts Institute of Technology (MIT). The calculated fission rates allowed the construction of two-dimensional radial maps of the DONJON5/BEAVRS deviations and two-dimensional mean values for the same deviations.

2. Benchmark for evaluation and validation of reactor simulations

The benchmark presents full description of the materials, geometry, core loading and detectors data for the first two cycles of operation of a four-loop Westinghouse nuclear reactor core.

This core has different types of fuel assemblies. Some assemblies bear burnable absorbers of Pyrex located in guide tubes spot. Throughout the rest of this article, the assemblies will be referred to according to their burnable absorber configuration. For example, the assembly with 6 Pyrex rods will be named "6BA" whereas an assembly without Pyrex will be named "0BA".

This work is about studying the impact of the homogenization of asymmetrical assemblies over the fission distribution, which makes the BEAVRS reactor particularly adapted for this type of study since it presents several configurations with no central symmetry. This is the case for assemblies 6BA and 15BA as depicted in Fig. 1. These assemblies are not splittable into identical eighth of an assembly and require a special processing for flux calculation and homogenization as described later in this paper.

The modeled configuration is the HZP case of the first cycle. The core has six different assembly geometries and three enrichments of ^{235}U. Its baffle width is about 2.22 cm. For the fission map computation, only the "All Rods Out" (ARO) case is studied. The physical state corresponding to this setup presents a thermal power of 25 MW_{th}, an inlet coolant temperature of 560 °F (566.5 K) and a critical boron concentration of 975 ppm.

For more details about the benchmark data, the reader can consult the BEAVRS specifications.

3. Initial two-level lattice calculation

In this section the lattice calculation options from the work of Canbakan and Hébert (2015) will be used.

3.1. Self-shielding

Self-shielding is performed using the *Subgroup Projection Method* (SPM) developed by Hébert (2009) and implemented in the DRAGON5 code. This method is based on CALENDF-type mathematical probatility tables, as proposed by Hébert and Coste (2002). This preferred method for DRAGON5 lattice calculation requires an energy mesh fine enough between 22.5 eV and 11.14 keV to get rid of the use of the slowing-down correlation effect inherent to the subgroup method. To this purpose, the SHEM361 (361 groups in energy) (Hébert and Santamarina, 2008) or the SHEM295 (295 groups in energy) are recommended. In this calculation scheme, the SHEM295 has been used.

The self-shielding step has been performed on an eighth of the assembly (see Fig. 2a), except for 6BA and 15BA assemblies which require to model the assembly in half. The water strip has been included in the outer cells. One can notice that the cladding/fuel pellet gap has been diluted inside the cladding to avoid numerical problems that could arise when treating a small area, and the four annular zones in the fuel pellet on Fig. 2b, following the recommendations of Santamarina et al. (2004) to compensate for the rim effect. In order to predict the plutonium buildup inside fuel pellets with more accuracy, ^{238}U is self-shielded both over the spatial and the energy domains. Whereas for the other isotopes, the

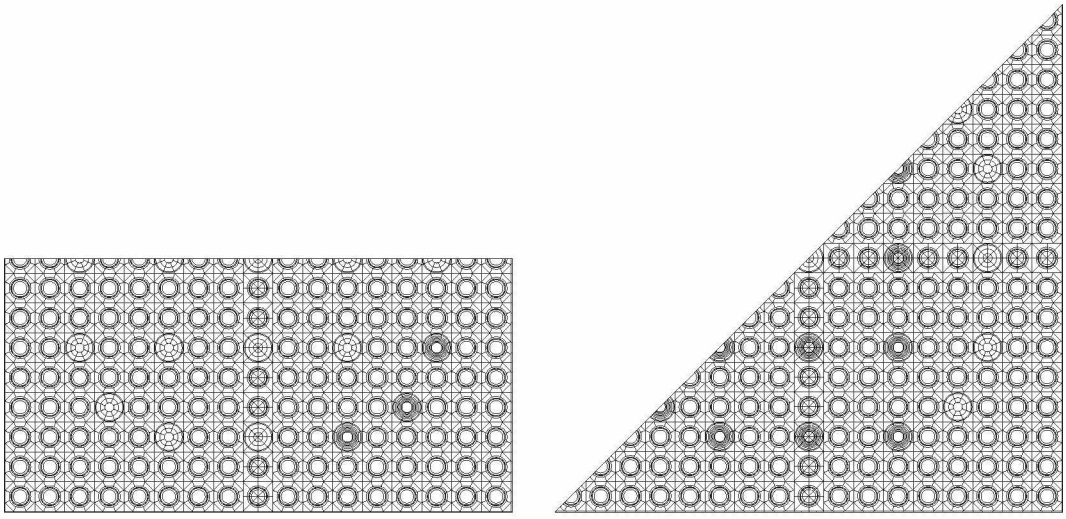

(a) 6BA (b) 15BA

Fig. 1. Second level flux calculation geometries for 6BA and 15BA assemblies. A splittable-in-two discretization has been adopted for the middle pins to allow several-area homogenization (cf. Fig. 4).

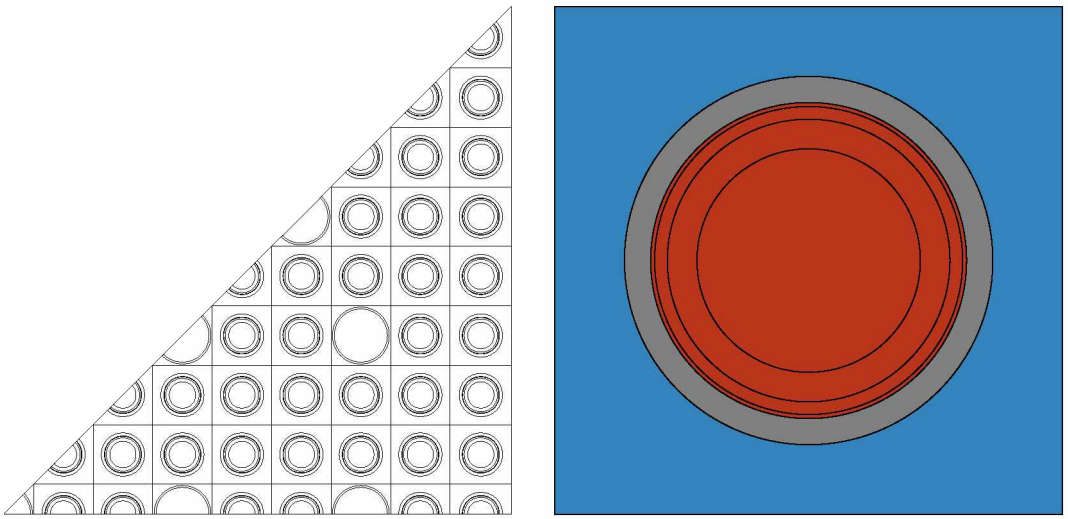

(a) Eighth of a 0BA assembly

(b) Fuel pin. Blue : moderator, gray : cladding and diluted cladding/pellet gap, red : fuel.

Fig. 2. Geometry for self-shielding calculation.

self-shielding is performed only over the energy domain and averaged over space in a fuel pin.

The following isotopes are self-shielded for energies above 4.63 eV: ^{235}U and ^{238}U for fuel, ^{90}Zr, ^{91}Zr, ^{92}Zr, ^{94}Zr, ^{96}Zr, ^{56}Fe and ^{52}Cr for structural materials such as burnable absorber cladding. The nuclear data used are from the JEFF-3.1.1 evaluation (Santamarina et al., 2009).

3.2. Flux computation

The flux calculation is performed in two steps on an eighth of an assembly, except for 6BA and 15BA assemblies which were modeled in half.

The first step is the flux computation using the interface current collision probability method (Sanchez and McCormick, 1982) with a zeroth order (P_0) development of scattering cross sections, and a double first order (double-P_1) decomposition of the angular flux at the interfaces (first order for the flux component following the normal vector to the interface, and first order for the flux component perpendicular to the normal vector to the interface). It is performed over a geometry quite similar to the one used for self-shielding, except for an additional annular region in the moderator around fuel pins, to account for better thermalization of neutrons (see Fig. 3a), and the separate modeling of the water strip for the outer pins of the assembly. This calculation is done over the 295 energy groups of the SHEM295 mesh with consideration of upscattering. The leakage coefficients are computed during this stage using a homogeneous B_1 leakage model, yielding one single homogeneous leakage rate per energy group, as detailed by Hébert (2020).

The second step consists in solving a k-eigenvalue problem for the neutron flux with a fixed leakage rate (as computed in the first stage), using the Method Of Characteristics (MOC) (Askew, 1972). Before operating the calculation, the cross sections are retrieved from the first step and condensed from 295 groups in energy to 26 groups. A superhomogénéisation (SPH) correction (Hébert, 1980) is applied to preserve reaction rates between the first flux calculation and the second to come. Regarding the spatial treatment of the cross sections, each volume is processed with its own local flux.

The computation is then carried out over a refined geometry ("windmill"-type mesh, see Fig. 3b). During this stage, the leakage coefficient is imposed and not recomputed due to the lack of precision of the energy mesh. It is retrieved from the first step and condensed over the 26 energy groups.

Following the second level calculation, a flux/volume type homogenization/condensation is implemented in order to obtain two energy groups cross sections for the core calculation. Since most assemblies have a central symmetry, the assembly is usually completely homogenized. In the case of assemblies 6BA and 15BA, the assembly can be homogenized by quarters in order to maintain a certain heterogeneity due to the arrangement of the Pyrex burnable absorber pins.

4. Modifications added to the lattice scheme

4.1. Homogenization, condensation

The homogenization step allows obtaining homogenized cross sections on full assemblies or on assembly quarters. Whichever option is chosen, we systematically represent the assemblies with homogeneous quarters in the core calculation, in order to compare homogenization methods, while all other things being equal. For most assemblies, these quarters are the same. However, in order to take into account the heterogeneity due to the different numbers of burnable absorbers between quarters, for assemblies 6BA and 15BA, those quarters can be homogenized differently. Consequently, three cases will be distinguished:

(A) half assembly lattice (Fig. 1) followed by several quarters homogenization (Fig. 4),
(B) half assembly lattice (Fig. 1) followed by complete homogenization,
(C) independent quarters (Fig. 5), homogenized independently.

Case A will be considered as the reference calculation given that it involves the fewest simplifying assumptions. This case will be the one studied for the majority of this paper, while cases B and C will be studied only in Section 6.3.

For those three cases, the homogenized cross sections were condensed to two energy groups, the energy cut-off being made at

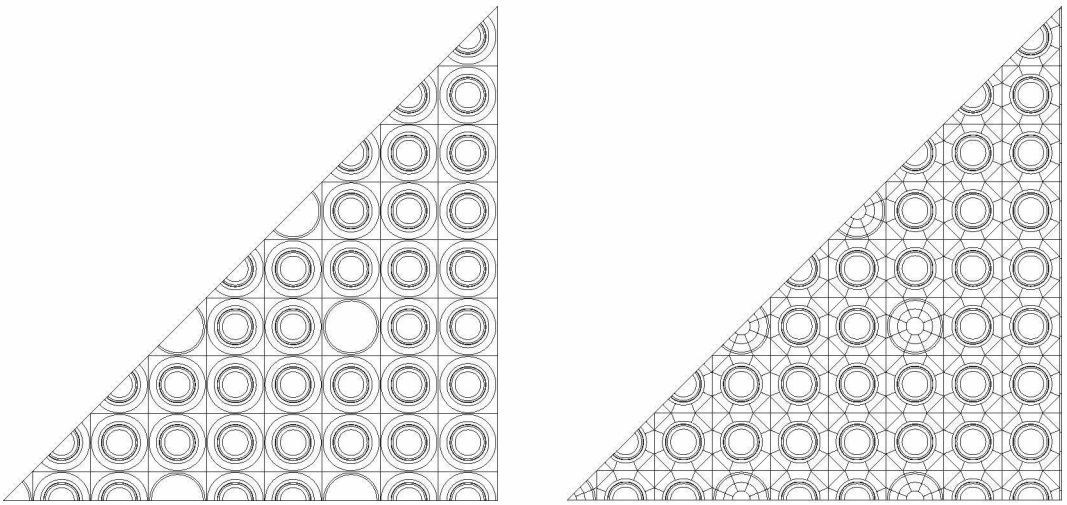

(a) First level flux calculation (b) Second level flux calculation

Fig. 3. Geometries of an eighth of a 0BA assembly for flux computation. Boundary conditions are symmetry for the diagonal and lower side, and reflection for the right side of the figures.

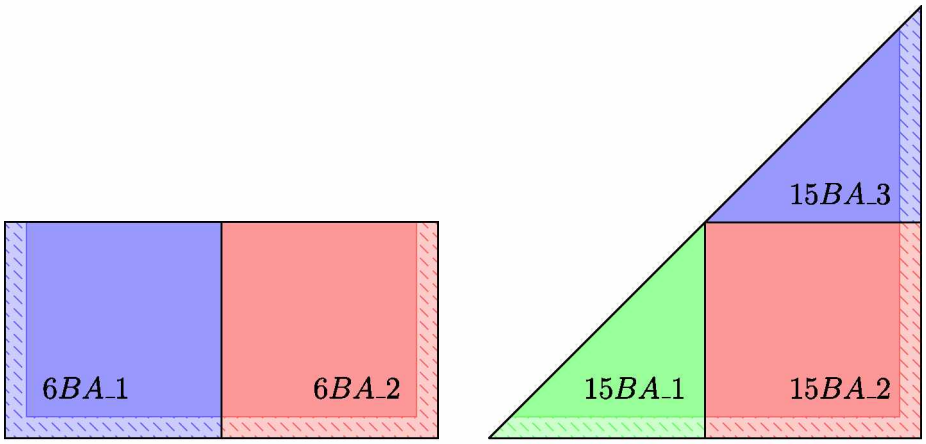

(a) 6BA (b) 15BA

Fig. 4. Homogenization areas for 6BA and 15BA assemblies (lighter, dashed area: water gap).

0.625 eV. In order to preserve the flux at the assembly boundaries during the core calculation, a Selengut type equivalence (Hébert, 2020) is implemented during this step. The homogenized cross sections are corrected by a multiplicative factor equal to the ratio of the surface flux in the water gap (hatched area on the Fig. 4)) to the average flux in the assembly.

4.2. Detectors model

The detectors used in BEAVRS are mobile fission chambers highly enriched in ^{235}U passed through empty guide tubes placed in the center of fuel assemblies. In DRAGON5 and DONJON5 codes, we modeled the detectors by a negligible concentration (using 10^{-10} atom $\cdot$ barn^{-1} $\cdot$ cm^{-1}) of ^{235}U in the water of those instrumentation tubes. The concentration must be low in order not to change the flux shape behavior. During the lattice calculation in DRAGON5, the cross sections of the detector isotope are then condensed and homogenized. Through this homogenization, we take into account the flux shape within the assembly (i.e., the flux in the guide tube) as proposed by Marleau et al. (2018) in module `EDI`. The microscopic cross section for reaction x and isotope i is written as

$$\bar{\sigma}_{x,i} = \frac{1}{\overline{N}_i \bar{\phi} \overline{V}} \int_{V_i} dV \int_{E_{\text{merg}}} dE N_i(\vec{r})\, \sigma_{x,i}(\vec{r}, E)\, \phi(\vec{r}, E) \tag{1}$$

where E_{merg} is the macro-group in energy over which the condensation is performed and $\overline{V}$ is the integrated volume, i.e., the value of the volume after homogenization, defined as

$$\overline{V} = \int_{V_{\text{merg}}} dV \tag{2}$$

where V_{merg} is the macro-volume over which the homogenization is performed.

The volume V_i is a subset of V_{merg} containing the isotope i and $\overline{N}_i$ is the number density for isotope i defined as

$$\overline{N}_i = \frac{1}{\overline{V}} \int_{V_i} dV N_i(\vec{r}) \tag{3}$$

where $\bar{\phi}$ is the integrated flux over E_{merg} and V_{merg}, written as

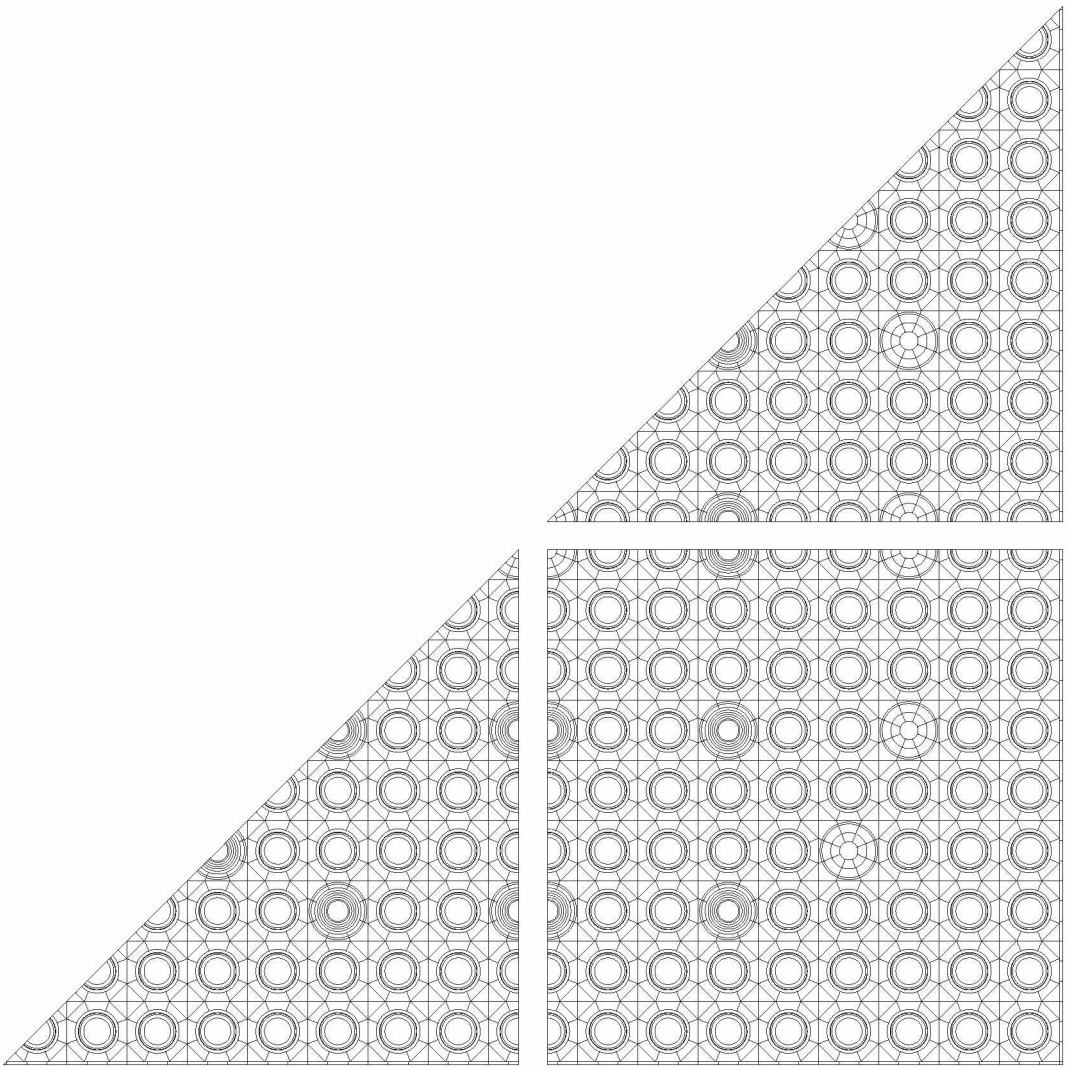

Fig. 5. DRAGON5 geometries for the three quarters calculations of assembly 15BA (second level of flux computation) for **homogenization case C**. Top right and bottom left quarter are modeled by an eighth of an assembly due to diagonal symmetry.

$$\bar{\phi} = \frac{1}{\overline{V}} \int_{V_{\text{merg}}} dV \int_{E_{\text{merg}}} dE \phi(\vec{r}, E) \tag{4}$$

where $\sigma_{x,i}, N_i(\vec{r})$ and $\phi(\vec{r}, E)$ are respectively the microscopic cross section, the number density of nuclei i and the scalar flux before homogenization and condensation.

5. Full-core calculation

5.1. Geometry

The whole core is modeled in the second step, with two energy groups, using the DONJON5 code. The assemblies are represented by homogeneous quarters. The four quarters are identical for assemblies with central symmetry but different for cases 6BA and 15BA, see Section 4.1. There are 31 planes defined along the z axis, two of them are composed solely of reflector materials (top and bottom). The remaining 29 are identical in height and content. The radial reflector shown on Fig. 6a is defined in the numerical model by a peripheral layer of assemblies as shown in Fig. 6b. The cross sections defining the reflector material are calculated according to different methods presented below. We neglected (i.e., not modeled) the grid spacers.

5.2. Reflector model

The equivalence methods used for the fuel are not applicable to the reflector, as these typically seek to preserve reaction rates and diffusion behavior. For an equivalent reflector, one rather wishes to preserve its reflective properties against an *external* neutron source. Various methods have been developed for this purpose. In this paper, we will compare the following methods:

- from Koebke et al. (1986) and
- from Lefebvre-Lebigot, as reported by Marguet (2018) and Richebois (1999).

Given the similarities between these two methods, their derivations are first developed jointly in 5.2.1, while the remainder are derived separately in 5.2.2 and 5.2.3. An alternative reflector model based on generalized perturbation theory (GPT) and mathematical programming was proposed by (Hébert and Leroyer, 2014).

5.2.1. Common approach

Both Koebke and Lefebvre-Lebigot methods are based on an equivalence between:

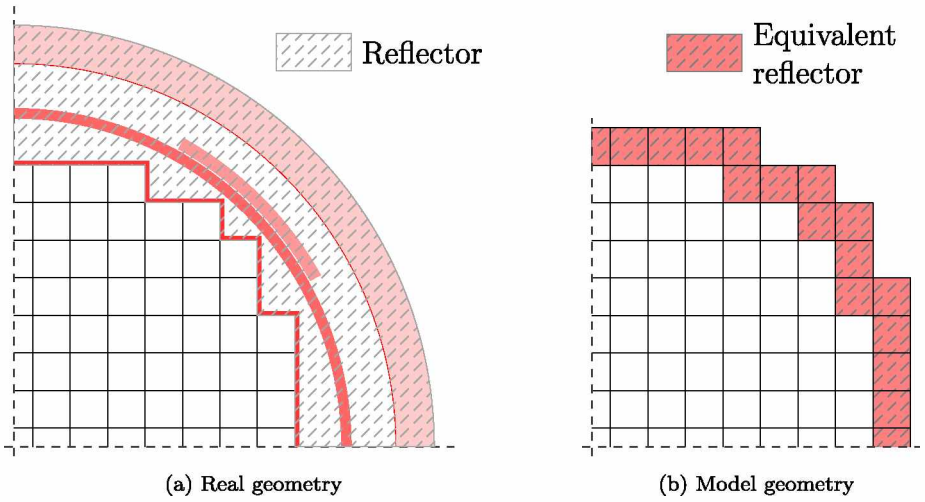

Fig. 6. Quarter core geometry.

(1) several hundred energy groups 1D transport carried out on a geometry representative of the interface between the core and the reflector (see Fig. 7a), and
(2) two energy groups analytical 1D diffusion on an equivalent homogeneous reflector (see Fig. 7b).

For the transport problem pointed in (1) on such a geometry (Cartesian, low dimensionality, deep), the discrete ordinates method is particularly efficient, with its mesh-to-mesh propagation. We use a high angular order (S_{16}) to capture the very anisotropic effects. It is necessary to choose a precise limit between the core and the reflector. To some extent, however, this choice is arbitrary. We may select a limit at the surface of the last fuel pin, a fictitious boundary in the water, or the inner surface of the steel baffle. We have chosen this latter solution, but this choice is open to debate and most often unmentioned.

The diffusion equations for the problem pointed in (2), i.e., on a 1D slab, with two groups, neglecting the upscattering, for a homogeneous and non-multiplying system, are written as

$$\begin{cases} -D_1 \frac{d^2\phi_1}{dx^2} + (\Sigma_{a1} + \Sigma_{1\to 2})\phi_1(x) = 0 \\ -D_2 \frac{d^2\phi_2}{dx^2} + \Sigma_{a2}\phi_2(x) = \Sigma_{1\to 2}\phi_1(x). \end{cases} \tag{5}$$

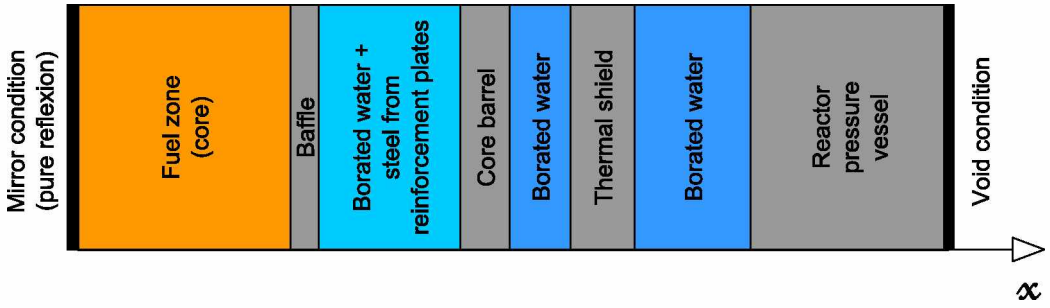

(a) Representative 1D model of a real reflector geometry. The fuel zone depth is the width of an assembly. The fuel properties are obtained by a classical homogenization (see 4.1) of any PWR assembly but without condensation.

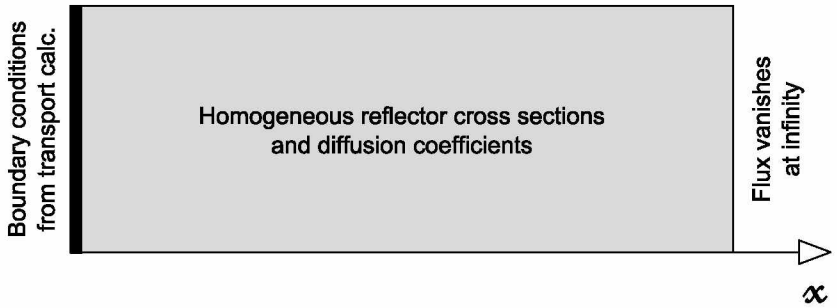

(b) Equivalent reflector model. The cross sections and diffusion coefficients of this area are unknowns that shall be determined through a reflector equivalence method.

Fig. 7. Representation of the reflector 1D radial models.

As a matter of fact, both Koebke and Lefebvre-Lebigot neglected reflector upscattering in their original methods. However, this approximation could be lifted without significant difficulty. The solution for the set of Eqs. 5 can be found analytically, considering an arbitrary flux on the left and a flux vanishing at infinity on the right. From this, an analytical expression of the current can also be derived. However the flux or current behavior *within* the equivalent reflector is irrelevant: we are only interested in the *interface between the core and the reflector*. At this location ($x = 0$) and for our case, one finds

$$\begin{cases} J_1 = \phi_1 \sqrt{D_1(\Sigma_{a1} + \Sigma_{1\to2})} \\ J_2 = \phi_2 \sqrt{D_2 \Sigma_{a2}} - \phi_1 \frac{\Sigma_{1\to2}\sqrt{D_1 D_2}}{\sqrt{\Sigma_{a2} D_1} + \sqrt{(\Sigma_{a1}+\Sigma_{1\to2})D_2}} \end{cases} \tag{6}$$

where J and ϕ are respectively the current and flux at the interface between the core and the reflector. We have dropped the signs indicating $x = 0$ to lighten the notation. All that remains is to define what exactly equivalent reflectors are.

5.2.2. Koebke's method

Koebke considers two reflectors as equivalent once they share the same R matrix as in

$$\phi_g = \sum_{g'} R_{gg'} J_{g'} \tag{7}$$

because it was noticed that this matrix was invariant for a given reflector, regardless of the fuel in front of it (for any fuel temperature, burnup, etc.). Two independent transport calculations are necessary and sufficient to calculate the elements of this matrix, since Eq. (7) becomes, for $g = 2$,

$$\begin{cases} \phi_2^A = R_{21} J_1^A + R_{22} J_2^A \\ \phi_2^B = R_{21} J_1^B + R_{22} J_2^B \end{cases} \Rightarrow \begin{cases} R_{21} = \frac{\phi_2^A J_2^B - \phi_2^B J_2^A}{J_1^A J_2^B - J_1^B J_2^A} \\ R_{22} = \frac{J_1^A \phi_2^B - J_1^B \phi_2^A}{J_1^A J_2^B - J_1^B J_2^A}. \end{cases} \tag{8}$$

For $g = 1$, Eq. (7) turns into

$$\phi_1 = R_{11} J_1 \tag{9}$$

so we could compute R_{11} with any of the two previous transport calculations (A or B) and obtain very similar results. To avoid a small variation due to the order of A and B, we use the average

$$R_{11} = \frac{1}{2}\left(\frac{\phi_1^A}{J_1^A} + \frac{\phi_1^B}{J_1^B}\right). \tag{10}$$

As can be seen with Eq. (8) by taking $A = B$, the two cases must be sufficiently different to avoid degeneracies. The exact choice of the neutron source does not matter: the only requirement is that two different spectra, representative of a PWR, are used to differentiate, in the reflector response, the thermal neutrons coming from the slowdown in the reflector (R_{21}) from those already emitted as thermal neutrons (R_{22}). As suggested by Marguet (2018), we use water in the fuel zone to have a large spectrum change. The water densities and the boron massic concentrations are, respectively,

(A) $\rho_{H_2O} = 0.55$ g/cm^3 with 500 ppm of boron, and
(B) $\rho_{H_2O} = 0.7$ g/cm^3 without boron.

Only the fuel change is considered while the reflector being characterized remains constant. In particular, the boron concentration *in the reflector water* is kept constant. These three known elements of R can be related to the five unknowns of the equivalent reflector cross sections ($\Sigma_{a1}, \Sigma_{a2}, \Sigma_{1\to2}$) and diffusion coefficients (D_1, D_2) through comparisons between Eqs. (6) and (7). Furthermore, Koebke chooses to add a sixth unknown, i.e., a discontinuity factor for thermal neutrons only, through the introduction of heterogeneous fluxes with $f_2 = \phi_2^{het}/\phi_2$ and $J_2 = J_2^{het}$. So we have three equations (from R) and six unknowns. To address this issue, Koebke proposes a flux-volume homogenization of the reflector region to set Σ_{a1}, Σ_{a2} and $\Sigma_{1\to2}$. Expressing the last three unknowns, one finds

$$\begin{aligned} D_1 &= \frac{1}{R_{11}^2(\Sigma_{a1}+\Sigma_{1\to2})} \\ f_2 &= \frac{-b \pm \sqrt{b^2 - 4ac}}{2a} \\ D_2 &= \frac{f_2^2}{R_{22}^2 \Sigma_{a2}} \end{aligned} \tag{11}$$

with

$$\begin{aligned} a &= \frac{\sqrt{(\Sigma_{a1}+\Sigma_{1\to2})}}{\sqrt{\Sigma_{a2}}} * \frac{R_{21}(\Sigma_{a1}+\Sigma_{1\to2}) - \Sigma_{1\to2}R_{22}}{R_{22}^2} \\ b &= \Sigma_{1\to2}\sqrt{D_1 \Sigma_{a2}} \\ c &= -R_{21}\Sigma_{a2} D_1 \sqrt{(\Sigma_{a1}+\Sigma_{1\to2})\Sigma_{a2}}. \end{aligned} \tag{12}$$

Up to now we have not found a situation in which $b^2 - 4ac \leq 0$ and we have always had two solutions. But curiously, the $+\sqrt{b^2 - 4ac}$ solution of f_2 is never mentioned in the literature (Koebke et al., 1986; Müller, 1991), even though it is a mathematically and physically viable solution (e.g. $f_2 > 0$). In practice, however, it leads to unreal power distributions. To our knowledge, this is the only reason to eliminate it. Finally, as suggested by Müller (1989), we incorporate f_2 discontinuity factor into cross sections and diffusion coefficients in a manner similar to a SPH equivalence with

$$\mu_2 = \frac{1}{f_2} \qquad \tilde{\Sigma}_{a2} = \mu_2 \Sigma_{a2} \quad \tilde{D}_2 = \mu_2 D_2. \tag{13}$$

5.2.3. Lefebvre-Lebigot's method

Through numerical transport experiments (see 5.2.1 point (1)), Lefebvre and Lebigot noticed that the ratio J_1/ϕ_1 (see Eq. (6)) is practically constant for a given reflector, whatever the fuel it faces. This parameter, computable by a transport calculation, is named

$$R_1 = \frac{J_1}{\phi_1}. \tag{14}$$

As for the ratio J_2/ϕ_1 (see again Eq. (6)), it varies for different fuels in an almost linear fashion as a function of ϕ_2/ϕ_1

$$\frac{J_2}{\phi_1} = R_2 \frac{\phi_2}{\phi_1} - R_3 \tag{15}$$

where R_2 and R_3 are respectively its slope and y-intercept opposite. Obviously, two distinct points (see Fig. 8) are necessary and sufficient to determine

$$R_2 = \frac{\phi_1^A J_2^B - \phi_1^B J_2^A}{\phi_1^A \phi_2^B - \phi_1^B \phi_2^A} \tag{16}$$

and

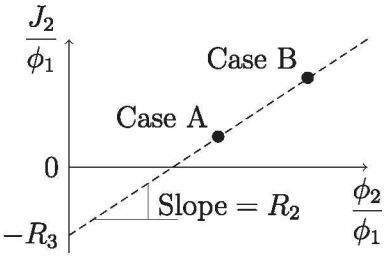

Fig. 8. Lefebvre-Lebigot's R_2 and R_3 can be determined from two points A and B by plotting J_2/ϕ_1 as a function of ϕ_2/ϕ_1.

$$R_3 = -\frac{J_2^A \phi_2^B - J_2^B \phi_2^A}{\phi_1^A \phi_2^B - \phi_1^B \phi_2^A}. \tag{17}$$

We use the same transport calculations (A and B) for Koebke and Lefebvre-Lebigot methods. Just like in Koebke's approach, these three known elements (R_1, R_2 and R_3) can be related to the five unknowns. For the last two unknowns, Lefebvre and Lebigot chose to set the reflector's diffusion coefficients to values close to those of the fuel in order to avoid large flux gradient discontinuities that could ruin the diffusion discretization. It is a common practice, as proposed by Lefebvre and Lebigot, to take

$$D_1^{\text{refl}} = 1.3 \text{ cm} \qquad D_2^{\text{refl}} = 0.4 \text{ cm} \tag{18}$$

because, for a PWR, we have

$$D_1^{\text{fuel}} \approx 1.3 \text{ cm} \quad D_2^{\text{fuel}} \approx 0.4 \text{ cm}. \tag{19}$$

At first sight, this choice may seem arbitrary. It is in fact as arbitrary as the homogenization proposed by Koebke to obtain Σ_{a1}, Σ_{a2} and $\Sigma_{1\to2}$. With the Eqs. (6), (14) and (15), we can express the other three unknowns as

$$\Sigma_{a2} = \frac{(R_2)^2}{D_2} \quad \Sigma_{1\to2} = R_3\left(\frac{R_1}{D_1} + \sqrt{\frac{\Sigma_{a2}}{D_2}}\right) \quad \Sigma_{a1} = \frac{(R_1)^2}{D_1} - \Sigma_{1\to2}. \tag{20}$$

5.2.4. Discussion

While the two approaches may seem quite different in their forms, a closer look at the Koebke and Lefebvre-Lebigot equations reveals that

$$\begin{aligned} \boldsymbol{\phi} &= R_K \boldsymbol{J} \\ \boldsymbol{J} &= R_{LL} \boldsymbol{\phi} \end{aligned} \tag{21}$$

and

$$R_K = R_{LL}^{-1} \tag{22}$$

with

$$\begin{aligned} \boldsymbol{\phi} &= \begin{pmatrix} \phi_1 \\ \phi_2 \end{pmatrix} \quad R_K = \begin{pmatrix} R_{11} & 0 \\ R_{21} & R_{22} \end{pmatrix} \\ \boldsymbol{J} &= \begin{pmatrix} J_1 \\ J_2 \end{pmatrix} \quad R_{LL} = \begin{pmatrix} R_1 & 0 \\ -R_3 & R_2 \end{pmatrix}. \end{aligned} \tag{23}$$

As can be seen, the two, Koebke and Lefebvre-Lebigot, methods lead to heterogeneous-homogeneous conservations. While Koebke method conserves the R_K matrix, the Lefebvre-Lebigot method conserves the inverse of R_K matrix, which is strictly equivalent. Their very few differences are exhaustively presented in Table 1. Although this would require further research, we suspect that almost all of the differences between the results of these two methods stem from the introduction of f_2.

5.3. Detectors response with module IDET

In order to compute the response of the modeled detectors described in Section 4.2, the module IDET recently implemented in DONJON5 is used. The positions of the detectors are provided to the module, and we perform an evaluation of fission chamber response by integrating the fission rate over the detector positions, as proposed by Hébert et al. (2019) in module IDET. In our case, each detector is located at the intersection of four assembly quarters. The flux is interpolated at the interface of each assembly quarter and then reaction rates are computed. However, the Raviart–Thomas polynomial solution is discontinuous at interfaces: there are actually four different reaction rates at the detector location (one for each quarter). To overcome this problem, the module IDET allows the user to define an area over which the calculated reaction rates are integrated. In this case the chosen area corresponds to the real detector area described in the benchmark specifications. The flux shape obtained in the lattice calculation is taken into account during the homogenization as described by the Eq. (1) in associated Section 4.2. This means that the exact position and volume of the detector are taken into account in spite of the homogenization applied to the whole (or quarter) assembly.

6. Numerical results

We strive to participate in reproducible research, so we've released our reflector, assemblies and full-core datasets in Salino (2020) and Fröhlicher (2020). Our results were obtained with version 5.0.5 (beta, revision 1761) of DRAGON5 and DONJON5 available from Marleau et al. (2018).

In this section we present the axially integrated fission rates obtained for the core calculation. In particular, we will compare:

- the minimal relative error,
- the maximum relative error,
- the Root Mean Square error (RMS_{2D}),
- DONJON5/BEAVRS relative error radial maps.

We focus on the root mean square discrepancy RMS_{2D}, defined as

$$RMS_{2D} = \left(\frac{\sum_{i=1}^{N} \left[\left(\sum_{z=1}^{N_z} R_{det,z}^{DONJON5,i} \right) - R_{det,2D}^{BEAVRS,i} \right]^2}{N} \right)^{\frac{1}{2}} \tag{24}$$

where $R_{det,z}^{DONJON5,i}$ is the detector response at height z (integrated over all N_z axial positions) and radial position i (N being the number of measurements available radially). $R_{det,2D}^{BEAVRS,i}$ is the axially integrated detector response published in the BEAVRS documentation.

The relative response error is defined as such:

$$\epsilon = \frac{\left(\sum_{z=1}^{N_z} R_{det,z}^{DONJON5,i} \right) - R_{det,2D}^{BEAVRS,i}}{R_{det,2D}^{BEAVRS,i}} \times 100 \tag{25}$$

Table 1
Differences between the Koebke and Lefebvre-Lebigot methods; from the point of view of the former since it introduces an additional degree of freedom (DoF), namely f_2.

Method	Unknowns	Fixed parameters	Value of the fixed parameters	Rationale
Koebke	D_1	Σ_{a1}	Reflector region flux-volume homogenization	Conservation of reaction rates in the reflector region
	D_2	Σ_{a2}		
	f_2	$\Sigma_{1\to2}$		
Lefebvre Lebigot	Σ_{a1}	D_1	1.3 cm	Avoid flux gradient discontinuities
	Σ_{a2}	D_2	0.4 cm	
	$\Sigma_{1\to2}$	f_2	1	Unintroduced DoF

6.1. Numerical quadrature effects

The diffusion solver is based on a mixed dual finite elements method. The geometry is discretized by the discretization module (TRIVAT module in DONJON5) and values are interpolated between the node by a polynomial function. The mass matrices used by the solver are computed by the same discretization module using either a Gauss–Lobatto quadrature (nodal type collocation) or a Gauss–Legendre quadrature (superconvergent finite elements). Here the impact on results is studied for these two quadratures and for two types of polynomials, quadratic and cubic. The reflector cross sections are computed with the Lefebvre-Lebigot method.

We notice on the Fig. 9 that the errors follow a checkerboard pattern. There is also a tilt between the center, where the discrepancies are negative, and the periphery of the core, where the discrepancies are positive. These effects appear in all the comparisons presented in this paper.

The results presented in Table 2 show better results when cubic polynomials are used. The use of parabolic polynomials does not allow satisfactory results as illustrated by RMS_{2D} of 7.39% and 7.98%.

Despite a theoretical decrease of precision due to a hollower matrix in the case of a Gauss–Lobatto quadrature, we obtain more satisfactory results with a RMS_{2D} lower than the one achieved for a Gauss–Legendre quadrature for both parabolic and cubic polynomials (see Table 2). This phenomenon is probably due to an error compensation that may occur in the calculation. As expected, cubic polynomials allow for better results. The checkerboard error pattern is less pronounced for the Gauss–Lobatto quadrature when used in conjunction with cubic polynomials, as illustrated in Fig. 9b.

6.2. Reflector model effects over errors

According to Table 3, the RMS_{2D} is lower, though of the same order, when the reflector is modeled by the Koebke method. The Koebke seems to be slightly better than the Lefebvre-Lebigot method as seen in Fig. 10a for which results are better than those presented on Fig. 9b. Nonetheless, the errors being of the same order of magnitude, this shows that both methods are suitable for this type of calculation.

While the results seemed improved by using a Gauss–Legendre quadrature with a Koebke reflector as seen in Table 3, Fig. 10b shows a degradation of the results, for which the checkerboard pattern is amplified compared to the results obtained with a Koebke reflector with a Gauss–Lobatto quadrature.

For the remainder of this article, the Koebke reflector with a Gauss–Lobatto quadrature and cubic polynomials are used.

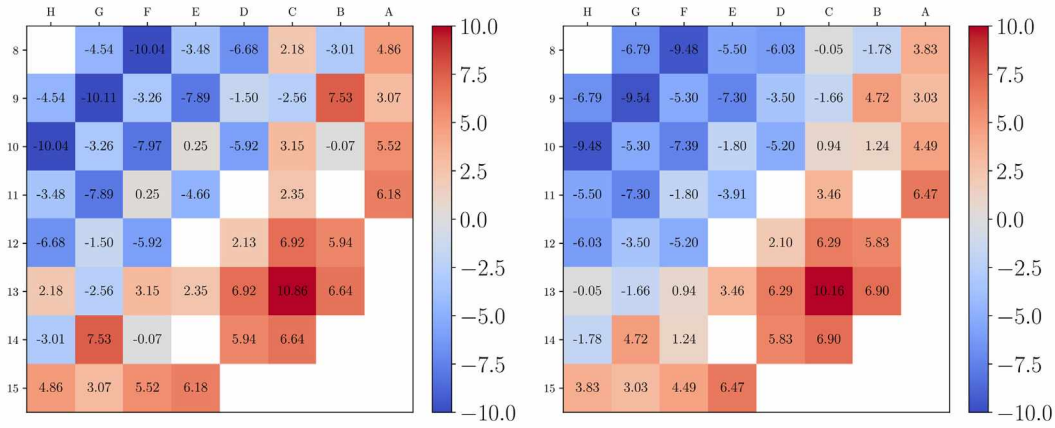

(a) Gauss-Legendre quadrature, cubic polynomials (DUAL 3 3)

(b) Gauss-Lobatto quadrature, cubic polynomials (DUAL 3 2)

Fig. 9. Fission rates relative discrepancies (%) between DONJON5 and BEAVRS measurements for Lefebvre-Lebigot reflector type.

Table 2
Numerical quadrature effects results.

Quadrature	Polynomials	Min (%)	Max (%)	RMS_{2D} (%)
Gauss-Lobatto	parabolic	−12.76	+12.46	7.39
Gauss-Legendre	parabolic	−15.52	+11.47	7.98
Gauss-Legendre	cubic	−10.11	+10.86	5.47
Gauss-Lobatto	cubic	−9.54	+10.16	5.22

Table 3
Reflector model and quadrature effects over global results (cubic polynomials).

Reflector method	Quadrature	Min (%)	Max (%)	RMS_{2D} (%)
Lefebvre-Lebigot	Gauss-Legendre	−10.11	+10.86	5.47
Lefebvre-Lebigot	Gauss-Lobatto	−9.54	+10.16	5.22
Koebke	Gauss-Legendre	−8.47	+8.37	4.46
Koebke	Gauss-Lobatto	−8.78	+8.49	4.66

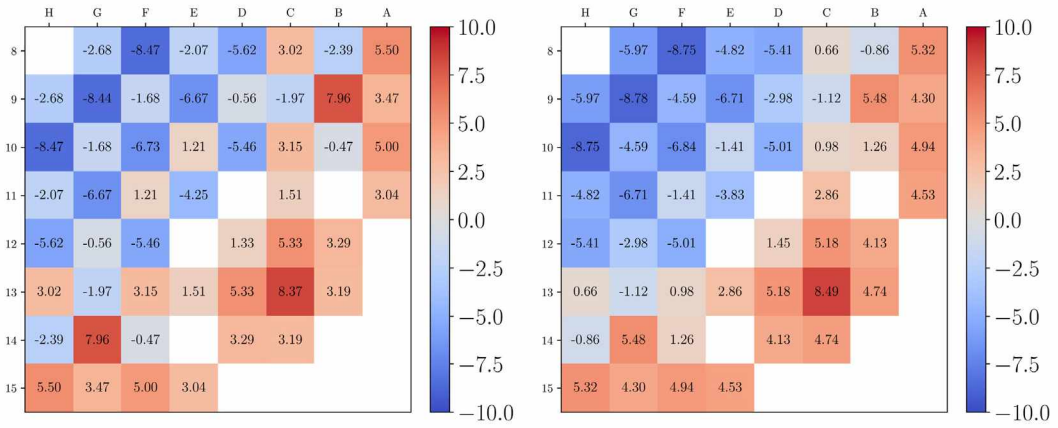

(a) Koebke reflector, Gauss-Lobatto quadrature (`DUAL 3 2`)

(b) Koebke reflector, Gauss-Legendre quadrature (`DUAL 3 3`)

Fig. 10. Fission rates relative discrepancies (%) between DONJON5 and BEAVRS measurements for Koebke reflector type (cubic polynomials).

Table 4
Quarter homogenization influence results.

Case	Min (%)	Max (%)	RMS_{2D} (%)
Homogenization case A (Ref.)	−8.78	+8.49	4.66
Homogenization case B	−14.28	+15.30	8.22
Homogenization case C	−8.51	+7.56	4.50

6.3. Homogenization for asymmetric assemblies

In this section, the comparison between the calculations performed with different cross section homogenization (cases A, B and C described in Section 4.1) is presented. As a reminder, results presented previously were obtained with case A homogenization.

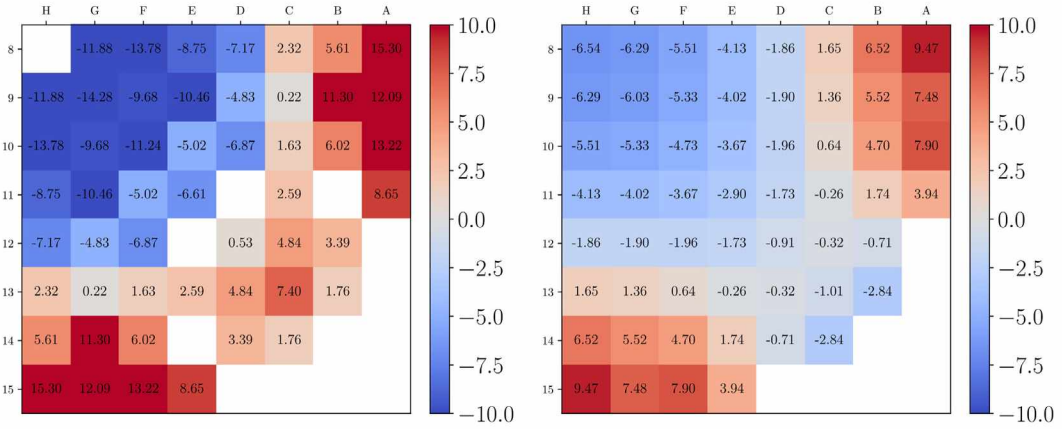

(a) Homogenization case B vs. BEAVRS data

(b) Homogenization case B vs. homogenization case A (reference)

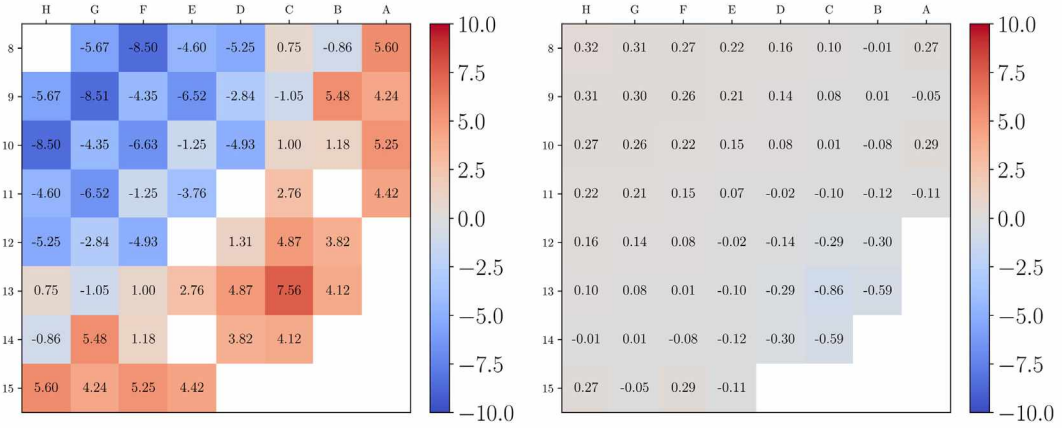

(c) Homogenization case C vs. BEAVRS

(d) Homogenization case C vs. homogenization case A (reference)

Fig. 11. Fission rates relative discrepancies (%) for different assembly homogenization.

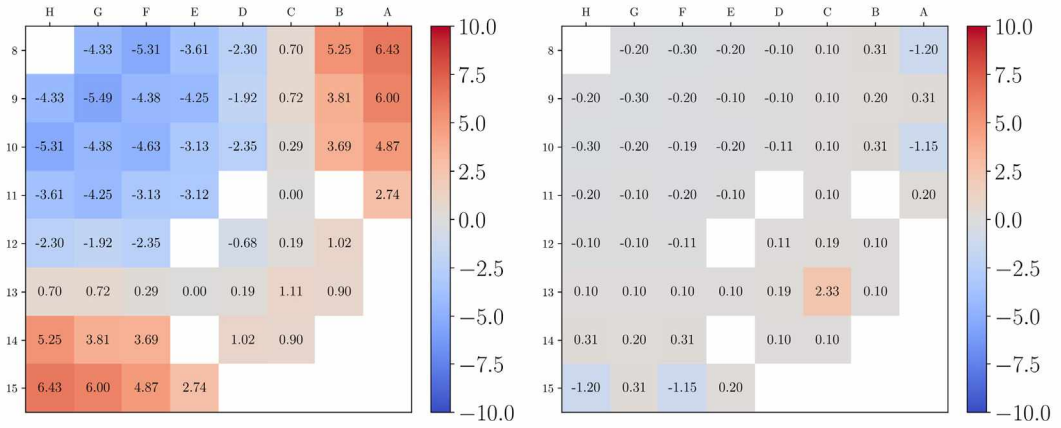

(a) Homogenization case B vs. homogenization case A

(b) Homogenization case C vs. homogenization case A

Fig. 12. Fission rates relative discrepancies (%) for different assembly homogenization with CASMO5/SIMULATE5 code sequence (retrieved from Bahadir, 2020).

Table 4 reports the differences observed on the radial fission rate map. Taking the heterogeneities into account makes it possible to improve the modeling significantly, -3.56% on the RMS_{2D} for homogenization case A compared to the homogenization case B with homogeneous assemblies, as well as an absolute decrease in the minimum and maximum deviations. In a recent paper (Bahadir, 2020), Bahadir obtains lower differences for the RMS obtained comparing calculation results to data provided in BEAVRS (-1.38% between cases A and B, and -1.45% between cases C and B) with CASMO5/SIMULATE5 code sequence. Fig. 11a shows that the maximum errors are located on the sides, whereas for the heterogeneous quarters case, the maximum error is located in the corner at the 15BA assembly location (see Fig. 10a). Fig. 11b shows the difference between several-area homogenization (case A) and complete homogenization (case B). One should note that the former method does not add computing time, hence leads to a significant improvement. The independent quarter modeling (case C) does not present so much difference with our reference (case A) as shown on Figs. 11c and 11d, respectively. The results obtained with CASMO5/SIMULATE5 show the same behavior between case A and case B (see Fig. 12a). As for the comparison between case A and case C, maximum discrepancies are still for 6BA and 15BA assemblies, but where DRAGON5/DONJON5 overestimates case C fission rates compared to case A, CASMO5/SIMULATE5 seems to underestimate them and vice versa. These conclusions come from Fig. 12b, which was reconstructed from data provided in Bahadir (2020).

6.4. Effective multiplicative factor

In this work, we chose to focus on the radial fission map. Nonetheless, the k_{eff} computed for the different reflector models and homogenization configurations were compared, and found to be relatively coherent. The maximum discrepancy is obtained between the homogenization cases B and C with $+155$ pcm for case B. Considering quarters in an infinite medium or inside their assembly environment (case C and A) only counts for 7 pcm. Finally, the reflector model did not change the result for more than 20 pcm.

7. Conclusion

The work described in this paper aims at presenting a full-core industrial-type calculation scheme for a PWR based on a transport/diffusion computation with the Canbakan and Hébert lattice scheme. It has been shown that DRAGON5/DONJON5 codes can perform HZP full-core calculation with less than 10% relative discrepancies over the radial fission map, corresponding to a radial RMS discrepancy of $\simeq 4.5\%$. Results in the Section 6.3 assess the effect of quarter homogenization for asymmetrical assemblies (like 6BA and 15BA for BEAVRS) on a full-core calculation. The orders of magnitude of the discrepancies observed in this article match the one calculated with CASMO5 and SIMULATE5 in Bahadir (2020). One should recall that taking into account those heterogeneities up to a certain extent (here quarter assembly scale) can significantly improve results over the whole assembly.

The best results were obtained using Koebke method for reflector treatment, a Selengut equivalence for the assemblies homogenization, as well as a Gauss-Laubato or Gauss–Legendre quadrature and cubic polynomials for the finite elements.

Finally, this work opens the path towards a more complex modeling of BEAVRS with DRAGON5 and DONJON5. It was not intent of this paper to model feedbacks and depletion mechanisms. However, modules are available in DONJON5 code to simulate those effects for future work on industrial PWR. It has also been shown that the flux tilt and fission map are significantly sensitive to the reflector model used. Improving those models, based on comparisons with Monte Carlo calculations, or using hybrid methods, could improve the results of the core calculation.

Declaration of Competing Interest

The authors declare that they have no known competing financial interests or personal relationships that could have appeared to influence the work reported in this paper.

Acknowledgments

This work was supported by a grant from the Natural Science and Engineering Research Council of Canada. We would like to thank the reviewers for their fruitful remarks about this work.

References

Askew, J.R., 1972. A characteristics formulation to the neutron transport equation in complicated geometries (AEEW-M1108), Transition to a Scalable Nuclear Future (PHYSOR 2020). .

Bahadir, T., 2020. BEAVRS benchmark evaluation with CASMO5 and SIMULATE5, Transition to a Scalable Nuclear Future (PHYSOR 2020). .

Canbakan, A., Hébert, A., 2015. Accuracy of a 2-level scheme based on a subgroup method for pressurized water reactor fuel assembly models. Ann. Nucl. Energy 81, 164–173.
Darnowski, P., Pawluczyk, M., 2019. Analysis of the BEAVRS PWR benchmark using SCALE and PARCS. Nukleonika 64, 87–96.
Fröhlicher, K., 2019. Mise en oeuvre d'un calcul du coeur BEAVRS en transport 3D cellule par cellule avec le code déterministe APOLLO3 (Master Thesis), Département de génie physique, École Polytechnique de Montréal. Montréal QC, Canada.
Fröhlicher, K, 2020. URL: https://gitlab.com/kfrohl/dragon-donjon-beavrs-modelling-frohlicher/-/tree/ANE2021.
Hébert, A., 1980. Développement de la méthode SPH: Homogénéisation de cellules dans un réseau non uniforme et calcul des parametres de réflecteur (PhD. Thesis).
Hébert, A., 1987. TRIVAC, a modular diffusion code for fuel management and design applications. Nucl. J. Canada 1, 325–331.
Hébert, A., 2009. Development of the subgroup projection method for resonance self-shielding calculations. Nucl. Sci. Eng. 162, 56–75.
Hébert, A., 2020. Applied Reactor Physics. Presses internationales Polytechnique.
Hébert, A., Coste, M., 2002. Computing moment-based probability tables for self-shielding calculations in lattice codes. Nucl. Sci. Eng. 142, 245–257.
Hébert, A., Leroyer, H., 2014. A presentation of the OPTEX reflector model. Nucl. Sci. Eng. 176, 312–324.
Hébert, A., Santamarina, A., 2008. Refinement of the Santamarina-Hfaiedh energy mesh between 22.5 eV and 11.4 keV. In: International Conference on the Physics of Reactors. Interlaken, Switzerland.
Hébert, A., Sekki, D., Chambon, R., 2019. A user guide for DONJON Version 5. Institut de génie nucléaire, Département de génie mécanique, École Polytechnique de Montréal. Montréal QC, Canada, Tech. Rep. IGE-344.
Horelik, N., Herman, B., Forget, B., Smith, K., 2013. Benchmark for evaluation and validation of reactor simulations (BEAVRS), v1. 0.1. Proc. Int. Conf. Mathematics and Computational Methods Applied to Nuc. Sci. & Eng, 5–9.
Koebke, K., Haase, H., Hetzelt, L., Winter, H.-J., 1986. Application and verification of the simplified equivalence theory for burnup states. Nucl. Sci. Eng. 92, 56–65.
Leppänen, J., Mattila, R., Pusa, M., 2014. Validation of the serpent-ARES code sequence using the MIT BEAVRS benchmark–Initial core at HZP conditions. Ann. Nucl. Energy 69, 212–225.
Marguet, S., 2018. The Physics of Nuclear Reactors. Springer.
Marleau, G., Hébert, A., Roy, R., 2018. A user guide for DRAGON Version 5, Institut de génie nucléaire, Département de génie mécanique, École Polytechnique de Montréal. Montréal QC, Canada, Tech. Rep. IGE-335. Homepage at URL: https://www.polymtl.ca/merlin/.
Müller, E.Z., 1989. Environment-insensitive equivalent diffusion theory group constants for pressurized water reactor radial reflector regions. Nucl. Sci. Eng. 103, 359–376.
Müller, E.Z., 1991. EQUIVA-2: a code for generating environment-insensitive equivalent nodal parameters for PWR reflector regions.
Park, H.J., Kim, S.J., Kwon, H. and Cho, J.Y., 2020. BEAVRS benchmark analyses by DeCART stand-alone calculations and comparison with DeCART/MATRA multi-physics coupling calculations, Nuclear Engineering and Technology.
Richebois, E., 1999. Calculs de coeurs REP en transport 3D, PhD. Thesis.
Salino, V, 2020. URL: https://github.com/IRSN/UncertaintyPhD/releases/tag/ANE2020.
Sanchez, R. and McCormick, N.J., 1982. A review of neutron transport approximations, United Kingdom Atomic Energy Authority.
Santamarina, A., Collignon, C., Garat, C., 2004. French calculation schemes for light water reactor analysis, The physics of Fuel Cycles and Advanced Nuclear Systems: Global Developments (PHYSOR 2004). .
Santamarina, A., Bernard, D., Blaise, P., Coste, M., Courcelle, A., Huynh, T.D., Jouanne, C., Leconte, P., Litaize, O., Mengelle, S. and others, 2009. The JEFF-3.1.1 nuclear data library, JEFF report, 22, 2..
Taforeau, J. and Salino, V., 2016. Analysis of the MIT BEAVRS Benchmark using the DRAGON-5/PARCS code sequence, Physics of Reactors, 1–5.
Vidal, J.-F., Litaize, O., Bernard, D., Santamarina, A., Vaglio-Gaudard, C. and Tran, R., 2007. New modelling of LWR assemblies using the APOLLO2 code package, Proc. Joint Int. Top. Mtg. on Mathematics & Computation and Supercomputing in Nuclear Applications (M&C+ SNA 2007), 15–19.
Vidal, J.-F., Fröhlicher, K., Archier, P., Hébert, A., Buiron, L., Palau, J.-M., Pastoris, S., Raynaud, D., 2020. New reference APOLLO3 calculation scheme for light water reactors – Analysis of the BEAVRS benchmark, Transition to a Scalable Nuclear Future (PHYSOR 2020).